RESONANT PIEZORESISTIVE AMPLIFIERS: TOWARDS SINGLE ELEMENT NANO-MECHANICAL RF FRONT ENDS

Alireza Ramezany[1], Sachin Babu[1], Varun Kumar[1], Jeong-Bong Lee[1], and Siavash Pourkamali[1]
[1]Electrical Engineering Department, University of Texas at Dallas, Richardson, Texas, USA

ABSTRACT

This work presents measurement and scaling results for micro/nano-mechanical resonant piezoresistive amplifiers (RPA) showing the potential of such devices as single element receiver front-ends. It has been previously demonstrated that the formation of an internal electromechanical positive feedback within a suspended resonant piezoresistor leads to a negative (active) motional resistance. Such devices can simultaneously amplify and filter incoming electrical signals while maintaining a low noise figure. Basic scaling physics suggests that by reducing the dimensions into the deep submicron range, RPAs can maintain similar negative motional resistances ($-r_m$), while consuming significantly less power and operating at higher frequencies. However, no empirical data has been shown to support this claim. In this work, RPAs with operating frequencies ranging from 5MHz to 162MHz have been fabricated and their performances have been compared. Measurements show a negative transconductance (g_m) of $-22mA/V$ ($r_m = -45\Omega$) with an effective quality factor of 2100 (in air) for a 162MHz RPA with DC bias power of only 530 µW. It is also shown that the figure of merit (FOM) for such devices (defined as g_m/P_{DC}) significantly improves by miniaturization of the resonant piezoresistor.

INTRODUCTION

Low-noise amplifiers and highly selective filters are crucial fundamental building blocks of any communication system. In the conventionally popular super-heterodyne front-end architectures, for example, the incoming RF signal from the antenna is filtered and amplified before being down-converted to an intermediate frequency (IF). The down-converted signal is further filtered and amplified and is sent to an ADC sampling at IF and eventually to digital signal processing units [1,2]. Due to the ever-growing need for speed and reliability of wireless communication technologies, addressing the complexity of RF systems is currently a much more daunting task than it was a decade ago. Today, there are multiple radios operating at the same time in a smartphone such as Cell Band, WIFI, Bluetooth, GPS, etc., as demonstrated in Figure 1a. RF front ends of current wireless systems also must often operate at different bands simultaneously [3,4]. Therefore, the need for adequate low noise amplification and filtering is more than ever.

With recent advancements in high frequency ADC technologies enabling sampling rates above 1 GSPS, the focus is shifting towards Direct Sampling at Radio Frequency. In this approach, the signal chain from the mixer onward is replaced with a high-performance RF sampling ADC, thus reducing the complexity of RF front ends (Figure 1b) [1,2]. In contrast to heterodyne architecture, the noise figure in the direct sampling approach is expected to be dominated by the ADC [1]. Even though the noise figure of modern RF sampling ADCs operating at 4GSPS can match that of IF sampling ADCs operating at 250MSPS (e.g. TI's ADC12J4000, ADS4149), additional gain from the IF amplifiers of the heterodyne architecture substantially reduces the impact of the ADC noise figure on the receiver sensitivity [1,4]. Therefore, the modern RF sampling ADCs require additional front end low noise amplification to reach the desirable performance [1].

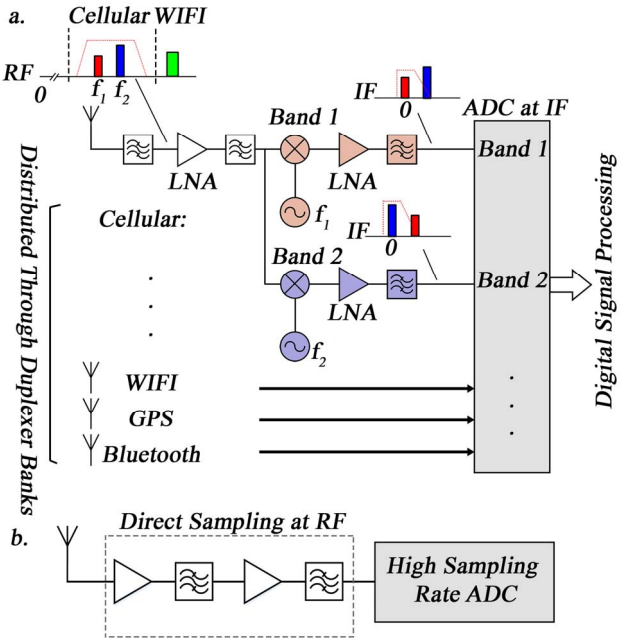

Figure 1. (a) Simplified schematic view of an RF receiver architecture, in which multiple radios operate with a similar architecture. An incoming signal is pre-filtered and amplified by a low noise amplifier (LNA) before being down-converted to a desired intermediate frequency. The IF signal is further filtered and transferred to ADC. (b) In direct RF sampling the entire signal chain from mixer onwards is eliminated. This necessitates low noise amplification to deliver the signal to ADC with an acceptable noise figure.

On the other hand, since the advent of the very first micromechanical resonator in 1967, the "Resonant Gate Transistor" [5], MEMS researchers have developed highly integrated on-chip timing and filtering technologies. However, the main bulk of recent research on micromechanical resonant devices has been focused on passive piezoelectric and capacitive resonators [6,7]. Such devices have not been able to meet the selectivity and pass-band loss requirements for wireless communications leading some researchers to turn the focus back to active on-chip resonant components, by combining field effect transistors or piezoresistivity with mechanical resonators [8,9].

One approach that takes such efforts one major step

further is the previously demonstrated thermal-piezoresistive internal amplification [10,11], in which a select frequency of the incoming signal is amplified and filtered at the same time through an internal electromechanical positive feedback of a resonant piezoresistive structure. This work investigates the effects of miniaturization on the performance of such devices.

THEORY OF OPERATION

Internal Amplification

Figure 2a shows the schematic view of the resonant structure comprised of a piezoresistive beam connected to two masses that can vibrate in an in-plane extensional mode. This resonance mode is excited when an AC signal at the resonance frequency is applied to the beam biased with a small DC current. The combination of the AC signal with the bias current creates a fluctuating component of input ohmic power (P_{ACin}). At resonance frequency, P_{ACin} creates temperature fluctuations T_{AC} in the beam, which through thermal expansion leads to a fluctuating stress σ_{AC}, amplified by the resonance and therefore a piezoresistive output signal.

However, if a beam with a negative piezoresistive coefficient, N-type doped silicon for example, is biased with a DC current it can create an internal electromechanical positive feedback that is capable of significantly increasing the vibration amplitude [10,11]. As more DC current is pumped into the system, a stronger internal power P_{int} is taken from the DC source to strengthen the internal feedback loop (figure 2b). In addition, while mechanical quality factor remains constant, the addition of P_{int} to the stored energy in the form of vibration raises the effective quality factor of the resonator to much higher (potentially orders of magnitude larger) values.

As demonstrated in [10], the resonant device can be modeled as a physical passive resistance R_A in parallel with a negative motional resistance ($-r_m = -1/g_m$) at resonance (figure 2c). Since the transconductance g_m is proportional to I_{DC}^2 [10], as the bias current increases and intensifies the internal amplification, it reduces the absolute value of the motional resistance $|-r_m|$. This trend continues until a negative overall device resistance ($R_D = R_A \,||\, -r_m$) is achieved. If loaded with a resistance R_L in the range of $-R_D/2 < R_L < -R_D$, the device can transfer an amplified version of the input signal to the load.

Scaling Physical Dimensions

Basic scaling physics suggests scaling down the dimensions can significantly improve the performance of the described resonant piezoresistive amplifiers. According to Eq. (1) [10,11],

$$g_m \propto {}^{1}/_{(f_0 C_{th})} \qquad (1)$$

where C_{th}, and f_0 are beam thermal capacitance and resonance frequency respectively. If the piezoresistive beam length and cross sectional area, along with the masses are scaled down by a factor of S, resonance frequency and thermal capacitance will be scaled by a factor of $s^{-1/2}$ and S^2, respectively. Therefore, the tansconductance g_m is expected to increase by a factor of $S^{-3/2}$ for the same DC

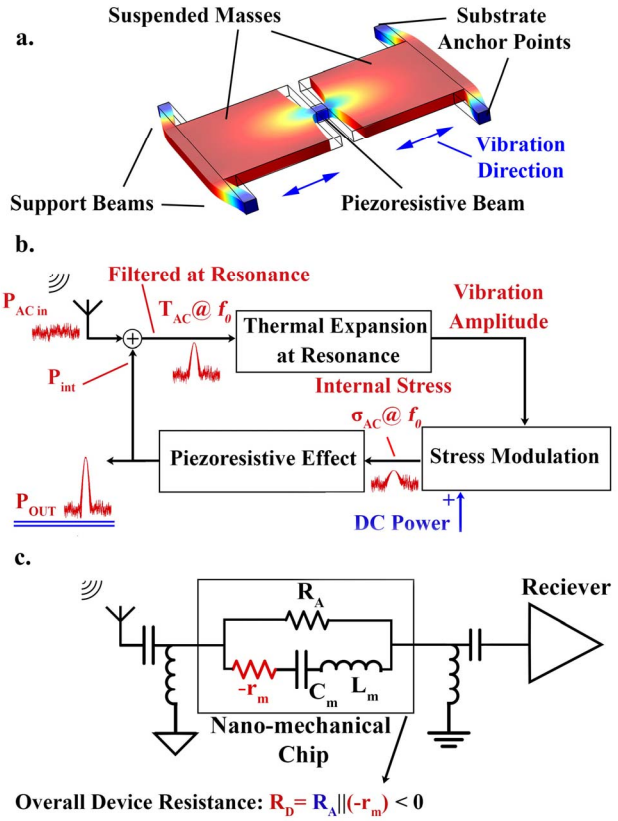

Figure 2. (a). Mode shape and the structure of an RPA (b) the positive piezoresistive electromechanical feedback leading to internal amplification. (c) The configuration of an RPA as an RF front end for a receiver with direct RF-sampling

power consumption [11]. This suggests an increase in the operating frequency alone without properly scaling down the beam dimensions (i.e., scaling down the masses much further than scaling the beam dimension) leads to deterioration of the transconductance. However, if the beam dimensions and the masses are scaled down simultaneously, it can potentially not only compensate for effect of frequency on the g_m but also improve the performance even more. This also implies that the same motional resistance, and consequently, the same level of gain (for the same load) can be achieved at a higher frequency in turn for a much less power consumption if the dimensions are scaled down.

FABRICATION

Fabrication of the resonant piezoresistive amplifiers requires a single lithography step on an SOI substrate followed by release of the silicon structure. To demonstrate the miniaturization behavior of the devices, a total of four devices were fabricated. Two low frequency devices operating at 5 and 10 MHz were first fabricated on an SOI substrate, with a 10µm thick device layer and 0.005 Ωcm resistivity. A standard photolithography capable of patterning minimum feature size of 2µm was used to pattern the devices and Si device layer was dry etched by DRIE. Beam dimensions of 6µm×0.5µm were then achieved via successive steps of dry thermal oxidation and oxide removal in hydrofluoric acid.

However, using this method to create smaller beam

dimensions is impractical. The thermal oxidation can reduce the width of the beam even down to nanoscale, but it increases the length of the beam in return. Therefore, to create beams that are shorter and thinner at the same time E-beam lithography is a more reliable approach.

Two more devices with much smaller dimensions, and resonance frequencies of 82 and 162 MHz were fabricated on an SOI substrate with 300nm thick device layer and average resistivity of 0.003 Ωcm. To reach deep submicron beam dimensions, E-beam lithography was performed on a 200nm thick 950 PMMA A4 resist. A 25nm Cr was deposited and lifted-off to form a hard mask. Chlorine based inductively coupled plasma (ICP) etcher was used to dry etch the Si device layer. The SEM images of all devices are shown in figure 3.

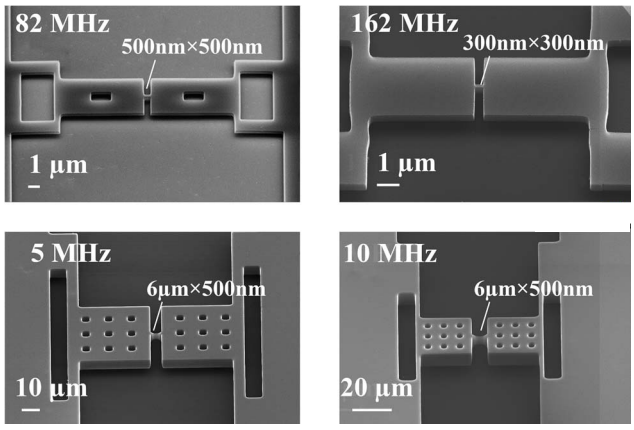

Fig 3. SEM views of the fabricated RPAs. The 82 and 162 MHz devices were fabricated using E-Beam Lithography, while the 5 and 10MHz were fabricated by standard photolithography.

MEASUREMENTS

As depicted in figure 4a, the S_{21} frequency responses of the devices were measured using a network analyzer. The changes in the response are monitored for various bias currents. Figure 4b, shows the measured frequency responses for the 5 MHz device measured in air, with various bias currents. As predicted in [11], for low bias currents, the P_{int}, the product of internal amplification, is not strong enough, and the motional resistance is very large in magnitude. Therefore, the device exhibits a passive behavior. As the current increases, the internal amplification intensified and the motional resistance value decreases in magnitude. As a result, a more dominant downward peak is observed.

With further increase in the bias current, the motional resistance compensates the passive physical resistance R_A (i.e., $r_m=R_A$, and $R_D \rightarrow -\infty$), and at the onset of active behavior, a very strong downward peak with 180º phase is attained. From this point forward, with more DC bias current pumped into the system, at resonance, the peak surpasses the feedthrough level, and eventually a power gain of unity is reached (i.e., $|R_D| = 2R_L$). The values for the effective quality factor, defined as $\Delta\omega_{-3dB}/\omega_0$, are mentioned in the plot showing the increase in the amount of internal power P_{int}, and internal amplification. Also, it should be mentioned that due to a small raise in DC temperature and reduction in Young's modulus, the

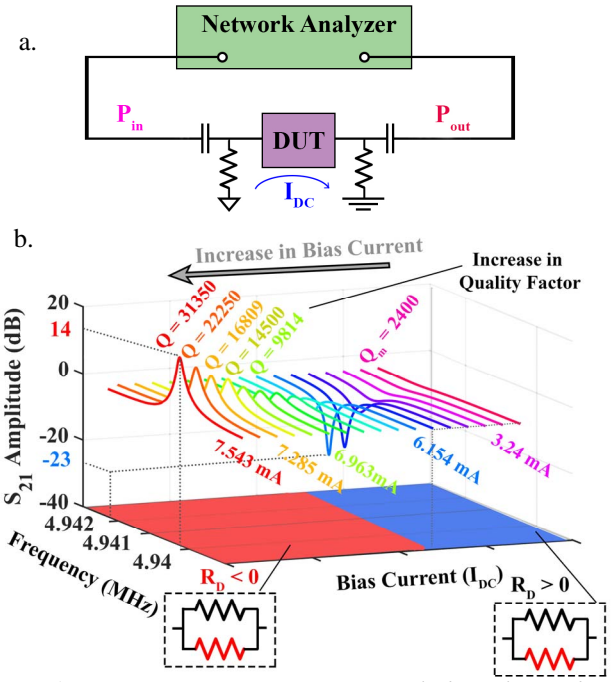

Fig 4. (a) Measurement setup including large bias resistors with 50 Ohm terminations on the network analyzer; (b) Measured S_{21} responses of the 5MHz Device with 50 Ohm load under atmospheric pressure.

resonance frequency slightly shifts towards lower frequencies.

Frequency responses of the devices with higher frequencies are expected to follow the same trend. Figure 5 shows the frequency response of the 162 MHz RPA measured under the same conditions. However, in this case, the effect of the parasitic capacitances are much more pronounced. For a more accurate comparison, the transconductance and motional resistances of all four devices were extracted from the measurements and plotted in figure 6. For the device operating at 162 MHz, motional resistances of lower than -50 Ohms (enough to provide gains for 50 Ohm loads) are achieved similar to those of the 5 MHz devices, but for an

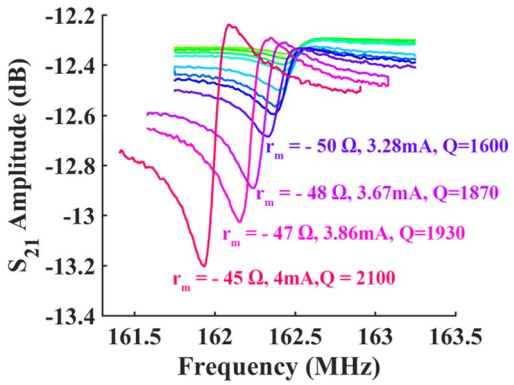

Fig 5. S_{21} response of 162MHz, the signal is limited by parasitic capacitances of the measurement setup.

almost four times smaller power consumption. This suggests that beam size miniaturization has not only compensated for the increase in frequency but also has improved the g_m.

Figure 7 shows the figure of merit defined as the ratio

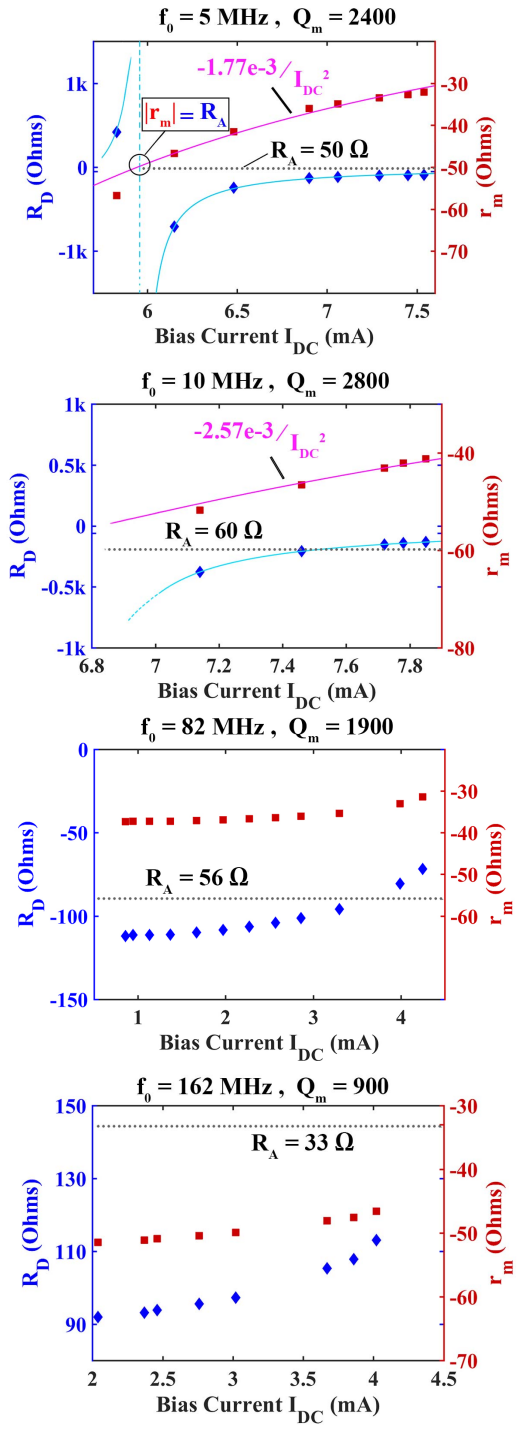

Fig 6. Measured device resistance R_D and motional resistance r_m vs. bias current for four different RPAs. As the bias current is increased r_m values reach the -50 ohm level, a value high enough to provide gains for a ~50ohm load. Despite increase in the frequency, as a result of miniaturization, the same r_m levels are achievable with lower device power consumption.

of transconductance g_m to the power consumption for the RPAs under study. Higher figure of merit values for higher frequency devices supports the notion that scaling the RPA dimensions even further, can potentially lead to high performance RPAs operting in the GHz frequency range suitable for communication applications.

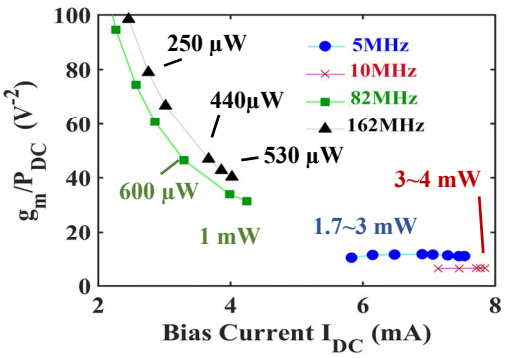

Fig 7. Figure of merit defined as the ratio of g_m to the power consumption. The larger FOM values for the miniaturized devices suggest significant improvement in RPA performances.

REFERENCES

[1] Neu, Tommy. "Direct RF conversion: From vision to reality." Texas Instruments, 2016.

[2] Lamontagne, Guillaume, and Ammar B. Kouki. "Direct RF sampling GNSS receiver design and jitter analysis." (2012).

[3] Ruby, Rich. "A Snapshot in Time: The Future in Filters for Cell Phones." *IEEE Microwave Magazine* 16.7 (2015): 46-59.

[4] Application Guide for Mobile Communication, Infineon, 2015, document reference number; AN_2015_06_PL32_002

[5] Nathanson HC, Newell WE, Wickstrom RA *et al.*, "*The resonant gate transistor*," *IEEE Transactions on Electron Devices* 1967; 14: 117–133.

[6] Nguyen, Clark T-C. "MEMS technology for timing and frequency control." *Proceedings of the 2005 IEEE International Frequency Control Symposium and Exposition, 2005.* IEEE, 2005.

[7] Piazza, Gianluca, Philip J. Stephanou, and Albert P. Pisano. "Piezoelectric aluminum nitride vibrating contour-mode MEMS resonators." *Journal of Microelectromechanical Systems* 15.6 (2006): 1406-1418.

[8] van Beek JTM, Phan KL, Verheijden GJAM *et al.* A piezo-resistive resonant MEMS amplifier. 2008 IEEE International Electron Devices Meeting; 15–17 Dec 2008; San Francisco, CA, USA; 2008: 1–4.

[9] Ansari A, Rais-Zadeh M. *A thickness-mode AlGaN/GaN resonant body high electron mobility transistor. IEEE Transactions on Electron Devices* 2014; **61**: 1006–1013.

[10] A. Rahafrooz, and S. Pourkamali, "High frequency thermally actuated electromechanical resonators with piezoresistive readout," IEEE Transactions on Electron Devices, vol. 58, no. 4, pp. 1205–1214, April 2011.

[11] A. Ramezany, M. Mahdavi & S. Pourkamali, "Nanoelectromechanical resonant narrow-band amplifiers", Nature Microsystems & Nanoengineering, Article number: 16004 (2016).

CONTACT

*A. Ramezany, Email: e.ramezany@utdallas.edu;